Scanned gate microscopy of surface-acoustic-wave-induced current through a depleted one-dimensional GaAs channel

R. Crook,* R. J. Schneble, M. Kataoka, H. E. Beere, D. A. Ritchie, D. Anderson, G. A. C. Jones, C. G. Smith, C. J. B. Ford, and C. H. W. Barnes

Cavendish Laboratory, 19 J J Thomson Avenue, Cambridge CB3 0HE, United Kingdom

(Received 15 July 2010; revised manuscript received 12 October 2010; published 29 October 2010)

We present scanned gate microscopy images of the surface-acoustic-wave (SAW)-induced current through a depleted GaAs one-dimensional channel. The images show a crescent-shaped feature, which splits into two fragments when the tip bias is taken more negative. This is consistent with depopulation of the SAW minima when the electron energy is out of equilibrium with the source two-dimensional electron system, where the maximum longitudinal potential gradient, along the length of the channel, sets a limit on the SAW-induced current. Part of a circular feature located near the channel exit is seen in the same images, which is probably caused by a low-amplitude reflected SAW with transport induced by a turnstile mechanism. Image analysis provides several parameters that are related to the electrostatic landscape at the channel entrance and are critical for controlling electron capture by the SAW potential. The parameters are the maximum potential gradient, the length of the channel entrance, and the precise location of the maximum potential gradient.

DOI: 10.1103/PhysRevB.82.165337 PACS number(s): 73.50.Rb, 07.79.−v, 73.23.Hk, 73.63.Kv

I. INTRODUCTION

Single electrons, or a small discrete number of electrons, can be trapped and transported in the potential troughs, or minima, associated with propagating surface-acoustic waves (SAWs).[1,2] This mechanism has the potential to deliver, manipulate, and extract single electrons from an otherwise isolated quantum device within the nanosecond timeframes required to study coherent electron dynamics.[3–5] The realization of more complex devices will require exquisite control of the electrostatic potential landscape throughout the device. Of particular importance is the potential landscape at the channel entrance, where electrons are captured from a two-dimensional electron system (2DES) and transferred to a depleted SAW-modulated channel, because the capture process both limits the SAW-induced current and determines the strength of current quantization.[6–12] Along the length of the channel it is essential to avoid puddles of electrons or current-limiting regions of high potential gradient because such irregularities are likely to disrupt coherent processes. Understanding the effect of the potential landscape has been largely limited to theoretical studies, being held back experimentally by the absence of spatially sensitive measurement techniques.

In this paper we demonstrate how scanned gate microscopy (SGM) can be used to modify and consequentially parametrize the electrostatic landscape of a SAW channel. This method could prove to be particularly useful for investigating long SAW channels or more complex prototype devices where unintentional potential irregularities may exist. SGM generates images by scanning a biased tip (the scanned gate) over a quantum device while an electrical property of the device is recorded to determine the shade of the spatially corresponding pixel in the image. Often the device conductance is recorded but in this case the SAW-induced current was also recorded. The biased tip locally perturbs the device potential landscape to modify the conductance or SAW-induced current as a function of the tip position. Using quantum devices without SAW-induced transport, SGM has previously been used to obtain unique spatial information about the device and tip potential landscapes and valuable insight in electron transport.[13–17] The SGM images presented here are compared with simulated images generated under the assumption that depopulation of SAW minima occurs when the electron energy is out of equilibrium with the source 2DES, following the observations and interpretation of Kataoka *et al.*[11] This interpretation means that the maximum potential gradient sets a limit on the SAW-induced current for a given SAW amplitude and channel width. The point of maximum potential gradient can be located either at the channel entrance or inside the channel. Three parameters are determined from the comparison. These are the maximum potential gradient, the length of the region where the maximum potential gradient occurs, and the position of the maximum potential gradient. In the case of this device, the last parameter confirms that the channel entrance is the current-limiting region and the first two parameters therefore characterize the potential landscape at the channel entrance.

II. EXPERIMENTAL METHOD

Figure 1 illustrates the experiment. A 2DES formed at a GaAs/AlGaAs heterojunction 90 nm beneath the surface with electron mobility 350 $m^2\ V^{-1}\ s^{-1}$ and electron density $3.7\times10^{15}\ m^{-2}$ after 1 s illumination with a red light-emitting diode. The SAW channel was defined from the 2DES by applying a negative bias to surface electrodes fabricated in a split-gate configuration. The channel was lithographically 2 μm long and 0.7 μm wide, with radii of curvature at the entrance and exit of 4 μm and 2 μm, respectively. This device was also used in an experiment to detect SAW-induced charging.[12] However, the channel electrostatic landscapes were not identical because the experiments were performed on different cryostat cooling cycles, which froze in slightly different configurations of donor charging. Device conductance was measured in the absence

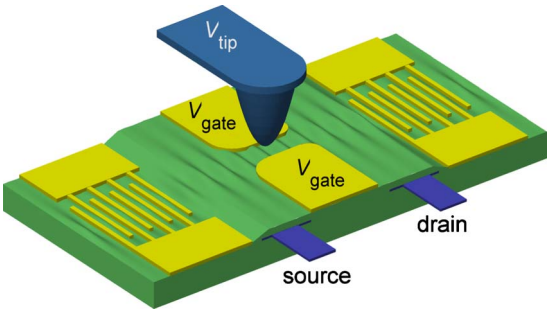

FIG. 1. (Color online) Illustration of experimental setup. SAWs are generated by applying a rf signal to the interdigitated transducer at the left end of the device. A negative bias applied to the central surface gates defines the SAW channel from the 2DES. Conductance and SAW-induced current measurements are made through the source and drain ohmic contacts.

of SAWs using standard lock-in amplifier techniques. A 0.2 mV ac excitation was applied to the source and the ac current measured from the drain.

SAWs, with a wavelength of 1.0 μm, were generated by applying a 2.7532 GHz radio-frequency (rf) signal to an interdigitated transducer which was fabricated over a region etched below the 2DES located 2.5 mm to the left of the SAW channel. A similar transducer, located at the right-hand end of the device, was unused but nevertheless acted as a Bragg reflector of the SAW.[18] The rf signal amplitude was 17 dBm but the signal reaching the transducer was attenuated due to losses in the cables and poor impedance matching between the cable and the transducer. To reduce sample heating and avoid interference between the outgoing SAW and either the free-space electromagnetic wave or reflected SAWs,[19,20] the rf signal was pulse modulated with a 1 μs width and a 4 μs period. The SAW-induced current was measured through the drain ohmic contact by the direct connection to a dc 20 V nA^{-1} transresistance amplifier, without a gating signal. A −0.3 mV dc bias was applied to the source ohmic contact to compensate for the amplifier input bias.

Atomic force microscopy was used to locate the surface electrodes defining the channel. Electrostatic force microscopy (EFM) was then used to accurately image the electronic outline of the electrodes. This technique detects changes in the mechanical resonance of the cantilever, which supports the tip, arising from the electrostatic force between the tip and the sample.[21] The EFM image shown in Fig. 2(a) was generated by applying an ac signal to the 2DES through both ohmic contacts while recording the amplitude of the cantilever mechanical oscillation. The force on the tip at the ac frequency ω is

$$F_\omega = -\left(\frac{\partial U}{\partial z}\right)_\omega = \frac{1}{2}\frac{\partial C}{\partial z}V_{dc}V_{ac},$$

where C is the capacitance between the tip and the 2DES and U is the energy stored in that capacitor, V_{dc} and V_{ac} are dc and ac parts of the potential difference between the tip and the 2DES, and z is the distance from the tip to the 2DES. When the tip is positioned over a surface electrode, which is held at a dc bias, C is reduced to almost zero due to screening of the 2DES by the electrode, so a reduced EFM signal identifies the presence of electrodes. The same spatial scanning parameters were used for all the images presented in this paper, so the same electrode outline can be accurately reproduced on all the images. The tip to sample separation was 50 nm.

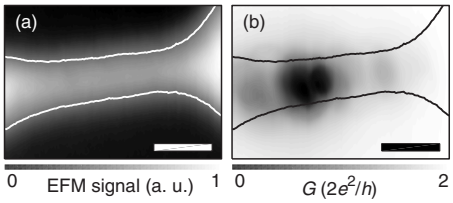

FIG. 2. (a) EFM image of the channel. The contour that has a channel width equal to the lithographic channel width is highlighted. The same contour is reproduced on subsequent images to locate the surface electrodes. (b) SGM image of conductance made with $V_{gate}=-0.6$ V and $V_{tip}=-2$ V. The image identifies the location and size of microconstrictions. Both images were made at 400 mK in the absence of SAWs. Scale bars are 1 μm.

III. SCANNED GATE MICROSCOPY IMAGES

The SGM image of device conductance, presented in Fig. 2(b), shows that the channel is not uniform but instead consists of a series of microconstrictions, or narrow regions, caused by electrode roughness, dopants, or defects. Following the method of Crook *et al.*,[22] based on the assumption of ballistic electron transport, SGM images can be calibrated to provide an approximate conduction-band-edge potential profile along a channel. The Fermi energy at the largest microconstriction is $E_F\ V_p/(V_b+V_p)$, where V_p is the minimum (absolute value) tip voltage required to take the device conductance to zero, V_b is the minimum (absolute value) tip voltage required to reveal all the local conductance minima and maxima in the SGM image, and E_F is the Fermi energy in the 2DES region. In this case, $V_p=-2$ V and $V_b=-0.9$ V so the Fermi energy at the largest microconstriction is $0.7E_F$ showing significant inhomogeneity in potential along the length of the channel. Although this image was necessarily made with the channel open at one conductive one-dimensional mode $(0<G<2e^2/h)$, a similar, but less well screened, potential profile will persist when the channel is depleted.

A sequence of SGM images, of SAW-induced current, is presented in Figs. 3(a)–3(c). As V_{tip} is taken more negative, a feature near the entrance (left-hand end) of the channel is seen to evolve from a spot, to a crescent, and then become disjointed. The SAW current associated with this feature is of the order $1ef$ or 440 pA. In all cases, the SAW current increases despite V_{tip} being negative. The images in Fig. 3 are markedly different from the image in Fig. 2(b), demonstrating that the SAW-induced current, unlike conductance, is not determined by the maximum potential. No strong structure is seen beyond the channel entrance, so in this case the potential landscape near the channel entrance determines the SAW-induced current through the entire channel. The images shown in Figs. 3(d)–3(f) are the same data used for the re-

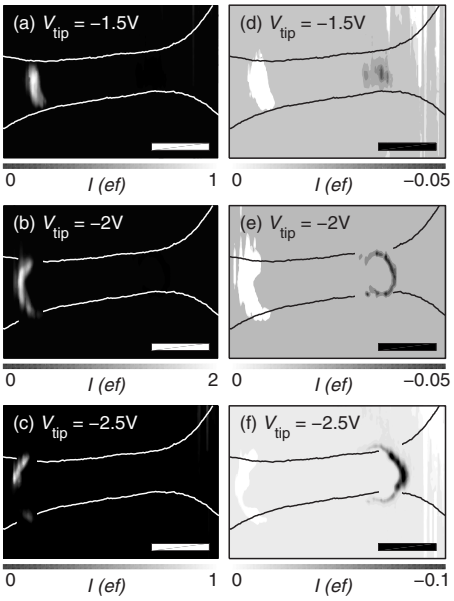

FIG. 3. Experimental SGM images of SAW-induced current. Before each image was generated, V_{gate} was adjusted so the background current was zero to remove the influence of the broad potential from the biased cantilever. Images (d)–(f) are enhanced versions of images (a)–(c), made by displaying only negative currents (charge flowing from right to left). All images were made at 400 mK in the presence of SAWs. Scale bars are 1 μm.

spective images in Figs. 3(a)–3(c) but only negative values of SAW-induced current are displayed. An additional feature is revealed near the exit of the channel, evolving from a spot to an almost complete ring as V_{tip} is decreased. In Fig. 3(e) there is also evidence of an outer ring. Note that the SAW current associated with the features near the channel exit, at about $0.05ef$ or 22 pA, is 20 times smaller than for the features near the channel entrance. The unused transducer acts as a Bragg reflector,[18] and because the SAW is pulsed, SAWs traveling from the two transducers arrive at the channel at different times, so avoiding interference. The features seen near the channel exit are likely to be caused by reflected SAWs.

IV. SIMULATION

To further investigate the origin and evolution of the crescent-shaped features, a numerical simulation was used to generate images. The one-dimensional potential profile along the length of the channel was modeled as

$$V(x) = \pm \alpha\beta/\pi \quad \text{when} \quad \pm x \geq \beta/2, \quad \text{and} \quad V(x) = (\alpha\beta/\pi)\sin(\pi x/\beta) \quad \text{when} \quad |x| < \beta/2.$$

Parameters α and β determine the maximum potential gradient in the channel entrance and the length of the channel entrance, respectively. This functional form was chosen as a model and is not based on theory or measurement. It is important to note that other continuous and smooth functional forms generate almost identical images. The tip was modeled as a charged sphere with a 0.15 μm radius. Figure 4 shows

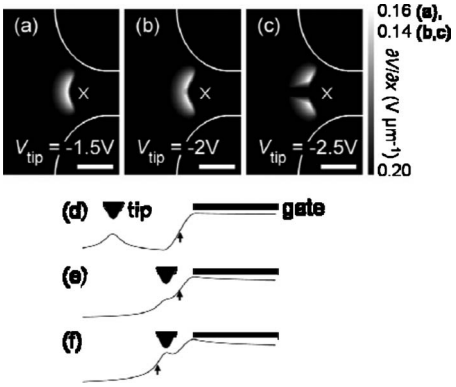

FIG. 4. [(a)–(c)] Simulated SGM images made by calculating the maximum potential gradient along the length of the channel in the presence of a negatively biased tip, plotted as a function of tip position. A cross locates the point of maximum potential gradient, in the absence of the tip perturbation. Scale bars are 1 μm. [(d)–(f)] Simulated potential at the entrance of the channel with the tip located (d) outside the channel entrance and in the channel entrance with (e) small and (f) large negative tip bias. Arrows indicate the maximum potential gradient in each case.

simulated images of the maximum positive potential gradient, $\partial V/\partial x$, along the length of a channel with the tip positioned at the spatially associated point of a 100×120 grid. The parameters, $\alpha=0.2$ V μm^{-1} and $\beta=0.8$ μm, were found to generate simulated images that most closely resembled the experimental images. Images generated with other values for α and β failed to reproduce the disjointed image seen in Fig. 3(c) and the correct feature evolution with V_{tip}. The curvature of the potential gradient, $V'''(0) = \alpha\pi^2/\beta^2 = 3.1$ V μm^{-3}, is less intuitive than β but is independent of the functional form.

The maximum potential gradient when the channel is conductive can also be calculated. By assuming that there is a linear relationship between device conductance and device potential, the SGM-image conductance profile along the center of the channel can be redrawn as the conduction-band-edge potential profile and calibrated using V_b and V_p. From the profile obtained from Fig. 2(b), the maximum potential gradient is measured as 6 mV μm^{-1}. The point of maximum potential gradient now lies within the channel, being associated with the disorder potential rather than the electrode potential. This significant reduction in the maximum potential gradient, and change in its position, is interpreted as the combined consequence of a less negative electrode bias and screening of the electrode and disorder potentials by 2DES electrons.

V. DISCUSSION

Theories propose that the depopulation of SAW minima occurs with the electron energy either in equilibrium[6,7] or out of equilibrium[8–10] with the source 2DES. Of the out-of-equilibrium models, the depopulation of the SAW-confined dots is suggested to be either by tunneling[8,9] or by thermal excitation.[10] For the out-of-equilibrium models, in the electron-capture region, the depth of the SAW-confined dots,

and therefore the SAW-induced current, is set by the potential gradient. For the in-equilibrium models, the local confining potential sets the SAW-induced current. A previous experiment using two channels in series concluded that the SAW-induced current is limited by the potential gradient in the channel entrance.[11] A different mechanism for electron capture, called the turnstile mechanism, occurs when the entrance and exit barriers of a Coulomb-blockaded (CB) quantum dot are modulated by the SAW potential.[23] The modulation is out-of-phase for the entrance and exit barriers, allowing electrons to be shuffled through the dot. This theory was used to interpret the observation of CB oscillations evolving into *nef* plateaus in SAW-induced current in the low SAW-power regime,[24] where f is the SAW frequency and n is the integer number of electrons in each potential trough.[1,2]

The similarity between the experimental and simulated images shows that the SAW current is being limited by the maximum potential gradient along the length of the channel, which is consistent only with an out-of-equilibrium theory to model SAW electron capture[8–10] and confirms earlier experimental reports.[11] Features in the images can be understood by considering the potential landscape that is the superposition of both the tip and channel potential functions. When $V_{\mathrm{tip}} \geq -2.0$ V, the maximum potential gradient is always associated with the channel potential function and, when the tip is remote as illustrated in Fig. 4(d), the potential gradient at the channel entrance is sufficiently high to inhibit all SAW-induced current, so the image background is zero. The crescent feature is created when the tip is positioned to the left of the channel entrance as illustrated in Fig. 4(e), where the negative potential gradient associated with the tip reduces the critical maximum potential gradient at the channel entrance enabling a nonzero SAW-induced current. When the tip is positioned to the right of the channel entrance, the maximum potential gradient will only increase, so it is impossible for the image to reveal a closed feature using this theory, which is consistent with the observations. When $V_{\mathrm{tip}} = -2.5$ V and the tip is positioned directly to the left of the channel entrance as illustrated in Fig. 4(f), the maximum potential gradient is now associated with the tip potential function. If the maximum potential gradient, to the left of the tip, is sufficiently large, the SAW-induced current is suppressed. This is the origin of the gap in the crescent feature seen in Figs. 3(c) and 4(c).

If the turnstile mechanism were responsible for transport in this device, then the images would reveal the superposition of ring features centered on a quantum dot, being similar to images from other Coulomb-blockade scanning-probe experiments.[14,16,25] This is because the capacitance between the tip and dot, and therefore the perturbation to the dot potential caused by the tip, depends upon the tip-to-dot separation but is independent of the tip-to-dot direction. While this is not the case for features seen near the channel entrance, the almost complete ring seen near the channel exit in Fig. 3(e) is likely to be caused by the turnstile mechanism with barrier modulation from the reflected SAW. Indeed, the reflected SAW has smaller amplitude than the forward-going SAW, and the turnstile mechanism was reported for the regime of small SAW amplitude.[24] It is likely that the quantum dot lies in series with regions of high potential gradient that normally prohibit reverse SAW current. In certain positions, the negatively biased tip will reduce the maximum potential gradient for reflected SAWs and permit a reverse current, as for forward SAWs. This second function of the tip potential may account for the incomplete imaging of the rings in Figs. 3(e) and 3(f). Evidence of an outer ring in Fig. 3(e) is consistent with transport through the next zero-dimensional subband within the quantum dot.

In this device, SAW-induced current quantization at integer multiples n of ef was not observed, despite the SAW-induced current being several times larger than ef. The absence of quantization is not unusual and is probably caused by poor lateral confinement in the channel, details of the potential landscape in the vicinity of the channel entrance, or the presence of microconstrictions, but the origin is not well established. SAW-induced transport is essential for the interpretation of these images, which clearly demonstrates that the absence of plateaus at *nef* does not rule out SAW-driven transport.

VI. CONCLUSION

We have presented scanned gate microscopy images of the SAW-induced current through a one-dimensional channel. By comparing experimental images with simulated images, the maximum longitudinal potential gradient is shown to set the limit on the SAW-induced current which is consistent with out-of-equilibrium SAW depopulation. This analysis also provides spatial parameters. For this device the maximum potential gradient was 0.2 V $\mu\mathrm{m}^{-1}$, the length of the channel entrance was 0.8 μm, and the precise location of the maximum potential gradient was identified. Circular features centered near the channel exit are understood to be caused by the low amplitude reflected SAW with transport induced by a turnstile mechanism.

ACKNOWLEDGMENT

This research was part of the QIP IRC (www.qipirc.org) supported by the U.K. EPSRC (Grant No. GR/S82176/01).

*Present address: Energy and Resources Research Institute, School of Process, Environmental and Materials Engineering, Faculty of Engineering, University of Leeds, LS2 9JT, UK.

[1] J. M. Shilton, V. I. Talyanskii, M. Pepper, D. A. Ritchie, J. E. F. Frost, C. J. B. Ford, C. G. Smith, and G. A. C. Jones, J. Phys.: Condens. Matter **8**, L531 (1996).

[2] T. J. M. Janssen and A. Hartland, Physica B **284-288**, 1790 (2000).

[3] C. H. W. Barnes, J. M. Shilton, and A. M. Robinson, Phys. Rev. B **62**, 8410 (2000).
[4] M. Kataoka, R. J. Schneble, A. L. Thorn, C. H. W. Barnes, C. J. B. Ford, D. Anderson, G. A. C. Jones, I. Farrer, D. A. Ritchie, and M. Pepper, Phys. Rev. Lett. **98**, 046801 (2007).
[5] M. Kataoka, M. R. Astley, A. L. Thorn, D. K. L. Oi, C. H. W. Barnes, C. J. B. Ford, D. Anderson, G. A. C. Jones, I. Farrer, D. A. Ritchie, and M. Pepper, Phys. Rev. Lett. **102**, 156801 (2009).
[6] K. Flensberg, Q. Niu, and M. Pustilnik, Phys. Rev. B **60**, R16291 (1999).
[7] P. A. Maksym, Phys. Rev. B **61**, 4727 (2000).
[8] G. R. A ĭ zin, G. Gumbs, and M. Pepper, Phys. Rev. B **58**, 10589 (1998).
[9] G. Gumbs, G. R. A ĭ zin, and M. Pepper, Phys. Rev. B **60**, R13954 (1999).
[10] A. M. Robinson and C. H. W. Barnes, Phys. Rev. B **63**, 165418 (2001).
[11] M. Kataoka, C. H. W. Barnes, H. E. Beere, D. A. Ritchie, and M. Pepper, Phys. Rev. B **74**, 085302 (2006).
[12] R. Crook, R. J. Schneble, M. Kataoka, H. E. Beere, D. A. Ritchie, D. Anderson, G. A. C. Jones, C. G. Smith, C. J. B. Ford, and C. H. W. Barnes, Phys. Rev. B **78**, 125330 (2008).
[13] M. A. Topinka, B. J. LeRoy, S. E. J. Shaw, E. J. Heller, R. M. Westervelt, K. D. Maranowski, and A. C. Gossard, Science **289**, 2323 (2000).
[14] M. T. Woodside and P. L. McEuen, Science **296**, 1098 (2002).
[15] R. Crook, A. C. Graham, C. G. Smith, I. Farrer, H. E. Beere, and D. A. Ritchie, Nature (London) **424**, 751 (2003).
[16] A. Pioda, S. Kičin, T. Ihn, M. Sigrist, A. Fuhrer, K. Ensslin, A. Weichselbaum, S. E. Ulloa, M. Reinwald, and W. Wegscheider, Phys. Rev. Lett. **93**, 216801 (2004).
[17] B. Hackens, F. Martins, T. Ouisse, H. Sellier, S. Bollaert, X. Wallart, A. Cappy, J. Chevrier, V. Bayot, and S. Huant, Nat. Phys. **2**, 826 (2006).
[18] M. R. Astley, M. Kataoka, C. J. B. Ford, C. H. W. Barnes, D. Anderson, G. A. C. Jones, I. Farrer, H. E. Beere, D. A. Ritchie, and M. Pepper, Phys. Rev. B **74**, 193302 (2006).
[19] R. J. Schneble, M. Kataoka, C. J. B. Ford, C. H. W. Barnes, D. Anderson, G. A. C. Jones, I. Farrer, D. A. Ritchie, and M. Pepper, Appl. Phys. Lett. **89**, 122104 (2006).
[20] M. Kataoka, C. J. B. Ford, C. H. W. Barnes, D. Anderson, G. A. C. Jones, H. E. Beere, D. A. Ritchie, and M. Pepper, J. Appl. Phys. **100**, 063710 (2006).
[21] C. Schönenberger and S. F. Alvarado, Phys. Rev. Lett. **65**, 3162 (1990).
[22] R. Crook, C. G. Smith, M. Y. Simmons, and D. A. Ritchie, Physica E **12**, 695 (2002).
[23] L. P. Kouwenhoven, A. T. Johnson, N. C. van der Vaart, C. J. P. M. Harmans, and C. T. Foxon, Phys. Rev. Lett. **67**, 1626 (1991).
[24] N. E. Fletcher, J. Ebbecke, T. J. B. M. Janssen, F. J. Ahlers, M. Pepper, H. E. Beere, and D. A. Ritchie, Phys. Rev. B **68**, 245310 (2003).
[25] R. Crook, C. G. Smith, W. R. Tribe, S. J. O'Shea, M. Y. Simmons, and D. A. Ritchie, Phys. Rev. B **66**, 121301(R) (2002).